Published online 20 November 2017

Nucleic Acids Research, 2018, Vol. 46, No. 1 ***431–441***
doi: 10.1093/nar/gkx1162

A *Thermus* phage protein inhibits host RNA polymerase by preventing template DNA strand loading during open promoter complex formation

Wei-Yang Ooi[1,†], Yuko Murayama[1,†], Vladimir Mekler[2,†], Leonid Minakhin[2,†], Konstantin Severinov[2,3,4,*], Shigeyuki Yokoyama[5] and Shun-ichi Sekine[1,*]

[1]RIKEN Center for Life Science Technologies, 1-7-22 Suehiro-cho, Tsurumi-ku, Yokohama 230-0045, Japan, [2]Waksman Institute of Microbiology, Piscataway, NJ 08854, USA, [3]Skolkovo Institute of Science and Technology, Moscow Region 143025, Russia, [4]St. Petersburg State Polytechnical Institute, St. Petersburg, Russia and [5]RIKEN Structural Biology Laboratory, 1-7-22 Suehiro-cho, Tsurumi-ku, Yokohama 230-0045, Japan

Received August 18, 2017; Revised November 01, 2017; Editorial Decision November 03, 2017; Accepted November 06, 2017

ABSTRACT

RNA polymerase (RNAP) is a major target of gene regulation. *Thermus thermophilus* bacteriophage P23–45 encodes two RNAP binding proteins, gp39 and gp76, which shut off host gene transcription while allowing orderly transcription of phage genes. We previously reported the structure of the *T. thermophilus* RNAP•σ^A holoenzyme complexed with gp39. Here, we solved the structure of the RNAP•σ^A holoenzyme bound with both gp39 and gp76, which revealed an unprecedented inhibition mechanism by gp76. The acidic protein gp76 binds within the RNAP cleft and occupies the path of the template DNA strand at positions –11 to –4, relative to the transcription start site at +1. Thus, gp76 obstructs the formation of an open promoter complex and prevents transcription by *T. thermophilus* RNAP from most host promoters. gp76 is less inhibitory for phage transcription, as tighter RNAP interaction with the phage promoters allows the template DNA to compete with gp76 for the common binding site. gp76 also inhibits *Escherichia coli* RNAP highlighting the template–DNA binding site as a new target site for developing antibacterial agents.

INTRODUCTION

Cellular gene transcription is accomplished by the multi-subunit DNA-dependent RNA polymerase (RNAP), through a multi-step process consisting of the initiation, elongation, and termination of transcription. Transcription initiation is the major control point of bacterial gene expression. The bacterial RNAP core enzyme consists of five subunits (α_2, β, β′ and ω), and assumes a 'crab-claw' shape. The binding of the dissociable σ subunit to the core enzyme forms the initiation-competent holoenzyme (α_2, β, β′, ω and σ) (1,2). The σ subunit plays a primary role during transcription initiation, and is subsequently ejected as RNAP proceeds towards the transcription elongation step (3). The principal housekeeping σ subunits (σ^{70} or σ^A) contain four evolutionarily conserved regions (the σ_1 – σ_4 regions/domains), which are further divided into several sub-regions. Within the context of the RNAP holoenzyme, the σ_2 region (sub-region $\sigma_{2.3}$) and the σ_4 region (sub-region $\sigma_{4.2}$) recognize and bind the –10 and –35 promoter sequence elements, respectively, which are located upstream of the transcription start site at +1, to form the closed promoter complex (RP_c) (4–6). Subsequently, a region of the promoter DNA (from *ca.* –12 to +2) is melted through interactions with σ and RNAP, and the RP_c transitions to the transcription-competent open promoter complex (RP_o) with the template DNA strand loaded into the RNAP active site (7–9). The $\sigma_{3.2}$ linker (sub-region $\sigma_{3.2}$) connecting the σ_3 and σ_4 domains lies on the inside of the RNAP DNA/RNA binding cleft, approaching the active site and occupying the RNA exit channel. The $\sigma_{3.2}$ linker forms direct contacts with the melted template DNA strand (7–9), and is responsible for complex isomerization from RP_c to RP_o (10).

Bacteriophages have evolved diverse mechanisms to control their bacterial host transcription machinery to favor their own developmental needs. P23–45, a bacteriophage that infects the thermophilic bacterium *Thermus thermophilus*, shuts off the host gene transcription upon infection (11,12). Similar to other phages, the P23–45 genes fall into three temporal expression classes. While the early

*To whom correspondence should be addressed. Tel: +81 45 503 9204; Fax: +81 45 503 9201; Email: shunichi.sekine@riken.jp
Correspondence may also be addressed to Konstantin Severinov. Tel: +1 848 445 6096; Fax: +1 848 445 5735; Email: severik@waksman.rutgers.edu
†These authors contributed equally to the paper as first authors.

genes are transcribed by a putative phage-encoded RNAP, the middle and late genes are transcribed by the host RNAP. P23–45 encodes two proteins, gp39 (a middle gene product) and gp76 (an early gene product), which bind to the host RNAP and strongly inhibit transcription initiation from the –10/–35 class of promoters, responsible for most of the host transcription (12). The inhibitory effects of the two proteins are weaker for the transcription of phage genes, which are driven by extended –10 class promoters, characterized by an extra sequence motif upstream of the –10 element but lacking the –35 element (12). We previously reported the structure of the *T. thermophilus* RNAP σ^A holoenzyme bound with gp39 (holo•gp39) (13). While the core domain of gp39 binds to the RNAP β-flap domain, which constitutes parts of the main channel and the RNA exit channel, the gp39 C-terminal tail binds and displaces the β-flap tip and the σ_4 domain. The drastic relocation of σ_4 is responsible for switching the promoter preference of the gp39-modified *T. thermophilus* RNAP: it impairs the recognition of the –10/–35 class promoters, but has a smaller effect on transcription from extended –10 promoters.

Similarly to gp39, gp76 alters the host RNAP preference by favoring transcription from phage promoters over host promoters (12), but the mechanism remains undefined. To elucidate how gp76 modifies the host RNAP function, we solved the crystal structure of the *T. thermophilus* RNAP holoenzyme bound to both gp39 and gp76. The structure revealed that gp76 binds deep within the RNAP cleft, in contrast to gp39, which binds to the rim of RNAP. The occupation of the main RNAP channel by gp76 and the interaction of gp76 with the $\sigma_{3.2}$ linker are incompatible with the DNA template strand binding to the same site. These results suggest that gp76 prevents the transition from RP_c to RP_o by blocking localized DNA melting and its propagation to the active site, thus compromising the functions of the σ_2/σ_3 regions of the σ subunit. The gp76 binding site is extensive and comprises evolutionarily conserved residues of the β, β′, and σ subunits. We show that gp76 also efficiently inhibits the non-cognate RNAP from *Escherichia coli*, and the mechanism of transcription inhibition is conserved. These results establish the RNAP cleft as a site for the development of compounds that target bacterial transcription.

MATERIALS AND METHODS

Protein preparation

The RNAP holoenzyme used for crystallization was purified from *T. thermophilus* HB8 cells, as described previously (14). The phage proteins gp39 and gp76 were expressed in *Escherichia coli*, and purified as described (12). For the preparation of the SeMet derivative of gp76, the single amino acid substitution of Met for Leu at position 13 (L13M) was performed, as gp76 only contains an N-terminal Met residue. To obtain the SeMet derivative of the L13M variant, *E. coli* cells bearing the expression vector were cultured in M9 medium containing SeMet (15). The His-tagged proteins were purified by chromatography on a HisTrap column (GE Healthcare), and then the N-terminal His-tags were removed by thrombin cleavage followed by another purification with the HisTrap column. The protein was further purified by Superdex75 gel filtration column chromatography (GE Healthcare).

Crystallization and soaking

For the co-crystallization of the *T. thermophilus* RNAP holoenzyme and gp39 (holo•gp39), the holoenzyme and gp39 were mixed in a ratio of 1:2. The protein mixture (1 μl, containing 23.5 μM holoenzyme and 47 μM gp39) was mixed with the equivalent volume of reservoir solution containing 45–50% tacsimate (pH 7.4), and crystallization was performed by the sitting-drop vapor diffusion technique. To obtain the crystals of holo•gp39•gp76, the native gp76 or the SeMet derivative of the L13M variant (final 25 μM) was added to the sitting drops containing the crystals of holo•gp39, and incubated for 1–4 day(s).

Data collection and structure determination

The X-ray diffraction dataset of holo•gp39•gp76 was obtained by using synchrotron radiation from the beamline BL41XU at SPring-8 (Hyogo, Japan) (Table 1). The diffraction dataset of holo•gp39•gp76 with the SeMet-containing L13M variant of gp76 was obtained at the beamline NE3A at the Photon Factory (Tsukuba, Japan). Reservoir solution plus 20% glycerol was used as the cryoprotectant for flash cooling in liquid nitrogen. The data were processed with the HKL2000 software package (16). The structure of holo•gp39 (PDB 3WOD (13)) was used as the search model for molecular replacement with the program PHASER (17). The resulting $F_o - F_c$ map revealed clear electron density for gp76 that was not present in the initial search model. The identification of two anomalous difference peaks from the data with the SeMet-containing L13M variant of gp76 confirmed that the electron density actually corresponds to gp76, and allowed model building of gp76 with the COOT program (18). After manual adjustment of the shifted regions, including the σ subunit, the β-flap, and gp39, the structure was refined with the PHENIX program (19).

SPR experiments

The binding affinities of gp76 for the *T. thermophilus* RNAP holoenzyme and core enzyme were estimated by the surface plasmon resonance (SPR)-based method by using a Biacore T200 system (GE Healthcare). The RNAP holoenzyme and core enzyme were immobilized on a CM5 sensor chip using the amine-coupling method at pH 5.5. The immobilized RNAPs were equilibrated with HBS-P buffer (10 mM HEPES-NaOH (pH 7.3), 150 mM NaCl, 0.05% Surfactant P20 (GE Healthcare)). gp76 was injected at concentrations of 0.045 to 2.88 μM over the holoenzyme, while 0.48 to 69 μM over the core enzyme. Data were analyzed by the BIAevaluation software using a 1:1 binding model. The dissociation constants (K_D) were calculated from equation $R_{eq} = (C \times R_{max})/(K_D + C)$, where C refers to the analyte concentration, R_{eq} to the binding response at equilibrium and R_{max} to the maximum binding response.

In vitro transcription

For *in vitro* transcription experiments, the 150–300 bp long promoter fragments containing three *T. thermophilus* HB8

Table 1. Data collection and refinement statistics

	Tth RNAP•σ^A•gp39•gp76	*Tth* RNAP•σ^A•gp39•gp76 (gp76 L13M SeMet)
Data collection		
Beamline	SPring-8 BL41XU	Photon Factory NE3A
Wavelength	1.000	0.978
Space group	$P3_221$	$P3_221$
Unit cell	$a = b = 294.4$, $c = 222.8$ Å $\alpha = \beta = 90$, $\gamma = 120°$	$a = b = 295.5$, $c = 221.6$ Å $\alpha = \beta = 90$, $\gamma = 120°$
Resolution range*	50–4.0 Å (4.15 – 4.00 Å)	50–6.0 Å (6.15–6.0 Å)
Reflections	92673 (9148)	54148 (3965)
Completeness	98.9% (98.1%)	99.7% (97.9%)
Mean I / σ	7.7 (1.8)	10.9 (1.3)
$CC_{1/2}$	0.993 (0.553)	0.992 (0.498)
R_{sym}	0.183 (0.724)	0.263 (2.092)
Redundancy	7.2 (5.2)	10.6 (10.3)
Refinement		
Resolution range	50–4.0 Å	
Reflections (work/test)	92624/4643	
R_{work}	0.2368	
R_{free}	0.2715	
RMSD		
Bond length	0.008 Å	
Bond angle	1.343°	
Ramachandran plot		
Favored	88.26%	
Allowed	10.98%	
Outliers	0.76%	

*Numbers in parentheses are for the highest resolution shell.

promoters (PrpoB1, PrpoB2 and PinfB) were obtained by PCR from genome DNA. The model T7 A1 and *gal*P1 promoters were PCR-amplified as 260 bp and 300 bp long DNA fragments from the plasmids containing the corresponding sequences. To monitor transcription elongation and termination, the promoter T7 A1 fused to a phage P23–45 intrinsic terminator t65 (20) was obtained by PCR from the corresponding plasmid.

Abortive transcription initiation reactions were performed in standard transcription buffer (30 mM Tris–HCl (pH 8.0), 40 mM KCl, 10 mM $MgCl_2$, 2 mM 2-mercaptoethanol), at 37°C for the *E. coli* RNAP σ^{70} holoenzyme and at 60°C for the *T. thermophilus* RNAP σ^A holoenzyme. The concentrations of the RNAPs and the promoter DNA fragment were 100 and 50 nM, respectively. The gp76 concentration was 1 or 4 μM. Promoter complexes were formed for 10 min at the respective temperatures. gp76 was added to the RNAP before or after the promoter DNA, as indicated. Transcription was initiated by the addition of 100 μM dinucleotide CpA and 20 μM UTP (in the presence of [α-^{32}P]-UTP), corresponding to the next promoter position, stopped after 5–10 min by the addition of an equal volume of urea–formamide loading buffer, and resolved on a 20% polyacrylamide denaturing gel.

Multi-round run-off transcription reactions by *T. thermophilus* RNAP σ^A holoenzyme were performed on a DNA fragment containing the T7 A1 promoter, in the standard transcription buffer at 60°C (Supplementary Figure S8A). The concentrations of the template, RNAP, and gp76 were the same as those in the abortive initiation reactions. The concentrations of gp39 were 1 and 4 μM. Promoter complexes were formed for 10 minutes, and reactions were performed for the next five minutes in the presence of 100 μM CpA and 50 μM ATP, 50 μM CTP, 50 μM GTP and 25 μM UTP (with the addition of [α-^{32}P]-UTP), stopped by the addition of an equal volume of urea–formamide loading buffer, and resolved on an 8% polyacrylamide denaturing gel.

Single-round transcription reactions were performed as described (20). Briefly, the transcription elongation complex (TEC) formed on the T7 A1-t65 promoter–terminator fusion (200 nM) and halted at position +20 of the template was prepared by performing transcription initiation with 100 nM *T. thermophilus* RNAP σ^A holoenzyme in the presence of a limited substrate set: 200 μM CpApUpC, 20 μM ATP, 10 μM CTP and 10 μM GTP (with the addition of [α-^{32}P]-GTP). The reactions were performed in the standard transcription buffer for 5 min at 60°C and then placed on ice. To prevent re-initiation, heparin was added to a final concentration of 0.05 mg/ml. To study transcription elongation and antitermination efficiency in the presence of the phage proteins, the halted TECs were supplemented with 5 μM gp39 or gp76 (where indicated) and incubated for 5 min at 60°C, followed by the addition of 50 μM NTPs. Aliquots were taken after 1–10 min, and the reactions were stopped by the addition of an equal volume of urea–formamide loading buffer, and resolved on an 8% polyacrylamide denaturing gel (Supplementary Figure S8B).

$KMnO_4$ probing

For *in vitro* $KMnO_4$ probing experiments (Figure 3C), PrpoB2 promoter was prepared from 90 nt long HPLC purified oligonucleotides (Integrated DNA Technologies) to comprise the double-stranded DNA fragment, corresponding to positions –56 to +34 with respect to the transcription

start site, as described (21). Either non-template (nt) or template (t) strand oligonucleotides were radioactively labeled with [γ-^{32}P]-ATP at their 5′ ends. Next, the labeled promoter fragments were purified on Micro Bio-spin 6 columns (BioRad) and used for the assays at 0.1 μM concentrations. Promoter complexes were formed in the standard transcription buffer without 2-mercaptoethanol in a final volume of 20 μl, and contained 0.2 μM *E. coli* RNAP σ^{70} holoenzyme, 5 μM gp76 (where indicated), and 0.05 μM of the DNA. Reactions were mixed with the order of addition of particular components as indicated, and incubated for 5 min at 37°C at each reaction step. Next, the promoter complexes were treated with 2 mM $KMnO_4$ for 40–60 s at 37°C. The reactions were ceased by the addition of 30 mM 2-mercaptoethanol, followed by ethanol precipitation and a 20 min treatment with 10% piperidine at 95°C. The reaction products were extracted with chloroform to remove the piperidine, ethanol precipitated, dissolved in 8 μl of urea–formamide loading buffer, and resolved on a 10% polyacrylamide denaturing gel.

Fluorometric assays

The RNAP holoenzymes containing the σ^{70} derivatives labeled either at position 211 with fluorescent 5-tetramethylrhodamine (TMR) (RNAP beacon) or at position 459 with fluorescein (RNAP-F) were prepared as described (22–24). To prepare gp76 labeled at the N-terminus with TMR, the protein was incubated with 5-carboxytetramethylrhodamine succinimidyl ester (Life technologies) in 0.1 M sodium bicarbonate buffer (pH 8.3) at room temperature for 3 h, and unreacted label was removed with a Bio-Spin 6 column (Bio-Rad). DNA oligonucleotides were synthesized by Integrated DNA Technologies. Fork junction and double-stranded DNA probes were prepared as described (23). Fluorescence measurements were performed using a QuantaMaster QM4 spectrofluorometer (PTI) in assay buffer (40 mM Tris–HCl (pH 8.0), 100 mM NaCl, 5% glycerol, 0.1 mM DTT and 10 mM $MgCl_2$) containing 0.02% Tween 20 at 25°C. Final assay mixtures (800 μl) contained 1 nM labeled RNAP holoenzyme and various concentrations of DNA probes. The TMR and fluorescein fluorescence intensities were recorded with excitation wavelengths of 550 and 490 nm and emission wavelengths of 578 and 520 nm, respectively. In beacon assay experiments, time-dependent fluorescence changes were monitored after manual mixing of the RNAP beacon (800 μl) and a DNA probe (<20 μl) in a cuvette; the mixing dead-time was 15 s. The complex of RNAP with gp76 was prepared by mixing 1 nM RNAP beacon with 150 nM gp76, followed by a 10 min incubation at room temperature.

RESULTS

Structure determination

The *T. thermophilus* P23–45 phage gp76 is a 5.8-kDa protein comprising 51 amino acid residues (Supplementary Figure S1). Crystals of *T. thermophilus* RNAP σ^{A} holoenzyme bound with both gp39 and gp76 (holo•gp39•gp76) were obtained by diffusing purified recombinant gp76 into preformed crystals of the gp39-bound holoenzyme (holo•gp39). A complete diffraction data set was obtained by using synchrotron radiation, and the structure was solved by the molecular replacement method, using the holo•gp39 structure (PDB 3WOD) as the search model (Figure 1A-C). The calculated electron density map clearly revealed the helical parts of gp76, and allowed the model building of gp76 (Figure 1D).

As the electron density was poor for the gp76 side chains, residue assignments were accomplished by using a selenomethionine (SeMet) derivative of the protein. Since wild-type gp76 contains only the N-terminal methionine residue, a leucine residue at position 13 was substituted with methionine, to add another SeMet location. X-ray diffraction data were obtained from a crystal soaked with the SeMet derivative of gp76 L13M. The Se anomalous difference peaks were identified for both SeMet residues (Supplementary Figure S2A), allowing precise model building.

No model was built for the C-terminal region of gp76 (residues 35–51), because the electron density for this region was missing. Thus, the final coordinates contain the N-terminal two-thirds of gp76 (residues 1–34), consisting of two α helices and their flanking loops (Figure 1A–D). Although the electron density for the σ subunit regions $\sigma_{3.0}$–$\sigma_{3.1}$ (the σ_3 domain (1)) was missing in the absence of gp76 (holo•gp39), it became partially visible in the presence of gp76 (holo•gp39•gp76), and coordinates were built for these regions (Supplementary Figure S2B). The refinement converged to final R and R-free factors of 0.237 and 0.272, respectively, at 4.0 Å (Table 1).

The gp76 structure and its binding site on the RNAP holoenzyme

The main body of gp76 is composed of two α helices (α_1, residues 6–16; α_2, residues 20–30), in good agreement with the secondary structure prediction (Figure 1A–D and Supplementary Figures S1 and S2). The α_1 and α_2 helices are joined by a short linker, and packed against each other in an anti-parallel fashion. The gp76 is bound deep inside the RNAP cleft, and docked in a space surrounded by the $\sigma_{3.2}$ linker, the β-flap, the β domain 1, a region following switch 3 (residues 1006–1031) in the β subunit, and the lid, rudder, and switch 2 regions of the β′ subunit (Figure. 1F). The $\sigma_{3.2}$ linker is one of the major binding sites of gp76, as an extensive network of hydrophobic interactions is formed between $\sigma_{3.2}$ (Ile321, Tyr329, Phe332, Ile333 and Pro334 (corresponding to *E. coli* σ^{70} Ile511, Leu519, Phe522, Ile523 and Glu524)) and gp76 (Val4, Ile9, Leu13, Phe27 and Ile31) (Supplementary Figures S3A and S4). The fact that the gp76 binding site is composed of multiple parts of RNAP explains why two-hybrid experiments failed to localize the gp76 binding site, while readily revealing the gp39 binding to the β-flap (20). The binding of gp76 resulted in a conformational change in the tip of the $\sigma_{3.2}$ linker, which shifted slightly away from the active site (Supplementary Figure S5).

gp76 is an acidic protein, and its surface is almost entirely negatively charged (Figure 1E). Besides the $\sigma_{3.2}$ linker, the α_1 helix also interacts with the region following switch 3 (residues 1006–1031) and switch 2 (Figure 1F and Supplementary Figures S3 and S4). Glu16 of gp76 potentially

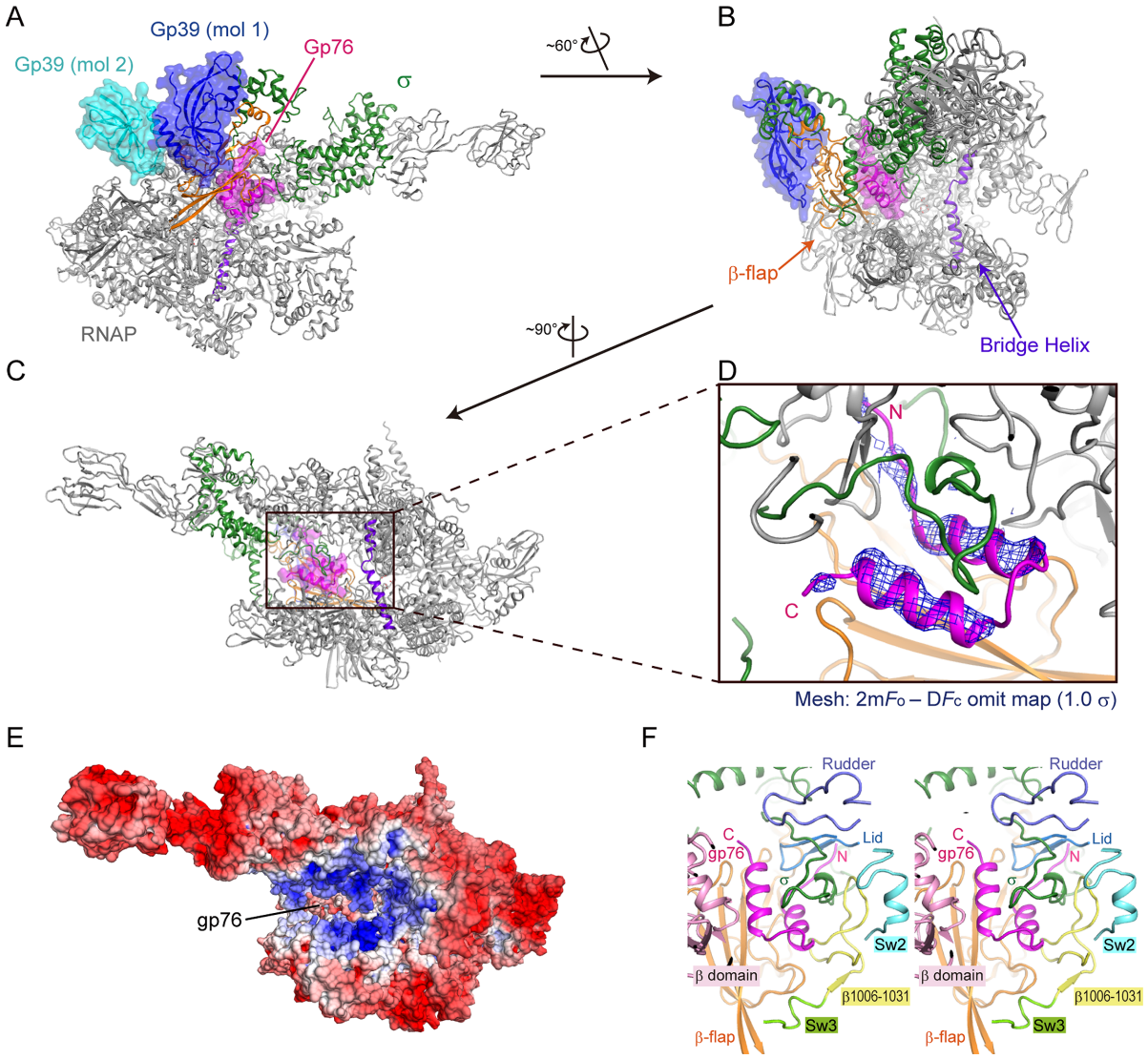

Figure 1. Structure of RNAP holoenzyme bound with gp39 and gp76. (**A**–**C**) Overall structure of the *T. thermophilus* RNAP σ^A-holoenzyme bound with gp39 and gp76 (holo•gp39•gp76) in three orientations. gp76, gp39, the σ^A subunit are colored magenta, blue, and green, respectively. The second molecule of gp39 is colored cyan. (**D**) A close-up view of the gp76 binding site. The $2F_o–F_c$ omit map calculated in the absence of the gp76 coordinates is overlaid with gp76, and contoured at 1.0σ. (**E**) The electrostatic potential distribution of the RNAP holoenzyme and gp76. (**F**) A stereo view showing the gp76 binding site.

forms electrostatic interactions with β′ Arg622 (Supplementary Figure S3B). The N-terminal loop of gp76 penetrates into the RNA exit channel, and is surrounded by the $\sigma_{3.2}$ linker, the β′ lid, and the β-flap. Glu7 of gp76 may interact with Arg713 and/or Arg758 in the β-flap (Supplementary Figure S3C). As compared with the holo•gp39 structure (13), the positions of the interlinked σ_4 domain of the σ subunit, the β-flap, and gp39 are shifted upon gp76 binding within the RNA exit channel (Supplementary Figure S5). The shift is slight, and the resulting position of σ_4 is still unfavorable for the recognition of the –35 element in the –10/–35 promoters.

The α_2 helix of gp76 resides in the RNAP main channel, and contacts the β domain 1 through potential electrostatic interactions between Glu22, Asp26, and Glu29 (gp76) and Asn130, Arg134, Arg383 and Arg388 (β domain 1) (Figure 1F and Supplementary Figure S3D). Although it is disordered, the C-terminal part of gp76 seems to extend toward the β′ rudder and the σ_3 domain. Probably because of the latter interaction, the electron density for the σ_3 domain, which was missing in the absence of gp76 (holo•gp39, (13)), became visible in holo•gp39•gp76. However, its orientation is slightly different from that in the free holoenzyme structure (1).

We measured dissociation constants of gp76 for *T. thermophilus* RNAP either in the form of the holoenzyme or core enzyme by SPR experiments (Supplementary Figure S6). While gp76 binds to the RNAP holoenzyme (RNAP•σ^A) with the K_D value of 0.12 ± 0.04 μM, it binds to the RNAP core enzyme with the K_D value of 8.4 ± 1.7 μM. This is consistent with the structural observation that the σ^A subunit forms a major interface with gp76. Despite

the higher K_D with RNAP core, gel shift analyses detected the gp76 binding not only to the RNAP holoenzyme, but also to the core enzyme (12), indicating that the electrostatic interactions between gp76 and the RNAP core (Figure 1E and Supplementary Figure S3B–D) are sufficiently stable to withstand electrophoretic separation.

In the holo•gp39•gp76 structure, the shelf module of RNAP is rotated or 'ratcheted' relative to the core module (25–27), and the clamp is in an open configuration, as compared with the holoenzyme (PDB 1IW7) and EC (PDB 2O5I) structures. This configuration is similar to that in holo•gp39 (13). However, our modeling indicates that gp76 binding is also compatible with an unracheted, closed-clamp conformation of RNAP, suggesting that the ratcheted, open-clamp configuration is not necessarily due to the gp76 binding.

gp76 occludes the DNA binding site required for the RP_o formation

Structural studies have revealed the detailed interaction points between DNA and the RNAP holoenzyme, which are crucial for the open bubble propagation during the RP_o formation (5,7–9,28). A superimposition of the holo•gp39•gp76 structure with that of *T. aquaticus* RP_o (PDB 4XLN (7)) is shown in Figure 2A–C. This view indicates that gp76 occludes the path for the melted DNA template strand, and the α_2 helix and the α_1–α_2 linker of gp76 clash with the DNA template strand at positions –11 to –4. In RP_o, the DNA template strand interacts with many basic residues, most of which are also close to gp76 (β Arg134, β Arg376, β Arg383, β Arg388, β Arg1031, β′ Arg622, Supplementary Figure S3). Thus, gp76 blocks the normal path of the template DNA strand, and should prevent the formation of RP_o (Figure 2A–C). The σ_3 domain, which is crucial for the –10 element recognition and DNA-strand resolution, changes its orientation by ∼15° upon gp76 binding (Figure 2B). This change could also affect the RP_o formation efficiency.

gp76 inhibits the RP_o formation

Based on the structural analyses presented above, gp76 binding should prevent the RP_o formation on the –10/–35 promoters. We examined inhibitory effects of gp76 on transcription by *T. thermophilus* RNAP. gp76 strongly inhibited abortive initiation from a –10/–35 promoter PrpoB2 (Figure 3A). Cumulative inhibitions by gp76 and gp39 were observed on –10/–35 promoters (Supplementary Figure S7), consistent with the distinct binding sites between gp76 and gp39. In contrast, almost no inhibition was observed for an extended –10 *gal*P1 promoter, in the presence of gp76, gp39 or both (Supplementary Figure S7). $KMnO_4$ probing revealed that gp76 indeed prevented promoter opening of the PrpoB2 promoter (Figure 3C).

Most *T. thermophilus* RNAP β, β′ and σ^A subunits residues that interact with gp76 are conserved in corresponding *E. coli* RNAP subunits (Supplementary Figure S4), suggesting that gp76 may also bind and inhibit *E. coli* RNAP. Indeed, we observed that gp76, unlike gp39, inhibited transcription initiation by *E. coli* RNAP σ^{70} holoenzyme from the PrpoB2 promoter similarly to *T. thermophilus* RNAP σ^A holoenzyme (Figure 3A). The *E. coli* holoenzyme forms a stable open complex on this promoter, and gp76 was ineffective when added after the promoter–complex formation (Figure 3B). Consistently, a $KMnO_4$ probing for the promoter complex formed by the *E. coli* holoenzyme revealed that only the addition of gp76 to the RNAP prior to the promoter DNA prevented promoter opening (Figure 3C). In contrast, transcription by the *T. thermophilus* holoenzyme was inhibited by gp76 whether added before or after the promoter DNA (Figure 3B), presumably because of the reversible nature of the open complexes formed by this enzyme (29,30).

These data suggest that gp76 cannot bind to a stable open promoter complex. To verify this, we monitored the gp76 binding to *E. coli* holoenzyme in the absence or presence of a promoter DNA by measuring FRET between a fluorescein probe incorporated in the σ^{70} subunit (residue 459, (24)) and a TMR probe attached to the N-terminus of gp76 (RNAP-F and gp76-TMR, respectively). A 100 bp DNA containing the N25cons promoter that forms a highly stable open promoter complex (21) was used in this experiment. Significant quenching of RNAP-F fluorescence (quenching efficiency = 0.31) was observed upon the addition of gp76-TMR (Figure 4), indicating that the RNAP-gp76 complex was formed. As expected, almost no change in fluorescence was observed when gp76-TMR was added to RNAP-F that was preincubated with the N25cons promoter DNA, indicating that gp76 indeed cannot invade a stable open complex, in which the DNA is already loaded.

The gp76 inhibition is based on competition with template DNA

To obtain additional evidence for the gp76 inhibitory mechanism based on competition with DNA for the same binding site, we investigated the interactions of *E. coli* RNAP with model promoter fragments by a fluorometric RNAP molecular beacon assay. This assay relies on the detection of the fluorescence signal from an RNAP holoenzyme derivative containing the σ^{70} subunit with a fluorescent label site-specifically incorporated in the proximity of the region $\sigma_{2.3}$, which recognizes the –10 promoter element (22,31). While the basal fluorescence of the RNAP beacon is low, it significantly increases upon specific RNAP beacon binding to a promoter DNA fragment (31). In Figure 5B, the fluorescence signal generated upon the addition of the T7 A1 promoter-containing DNA fragment to the RNAP beacon preincubated with gp76 is considerably lower than that observed in the absence of gp76. This result indicates that gp76 inhibits the formation of the RNAP–promoter complex, consistent with the abortive transcript synthesis experiments (Supplementary Figure S7). Thus, the beacon assay allows the monitoring of the inhibitory action of gp76 on RNAP–promoter interactions. The structural data suggest that gp76 hinders the RNAP interactions with the template strand segment of the transcription bubble, while not significantly influencing RNAP binding to the promoter segment upstream of the –10 element or to the non-template strand segment of the –10 element. Therefore, we measured the effect of gp76 on *E. coli* RNAP beacon binding to pro-

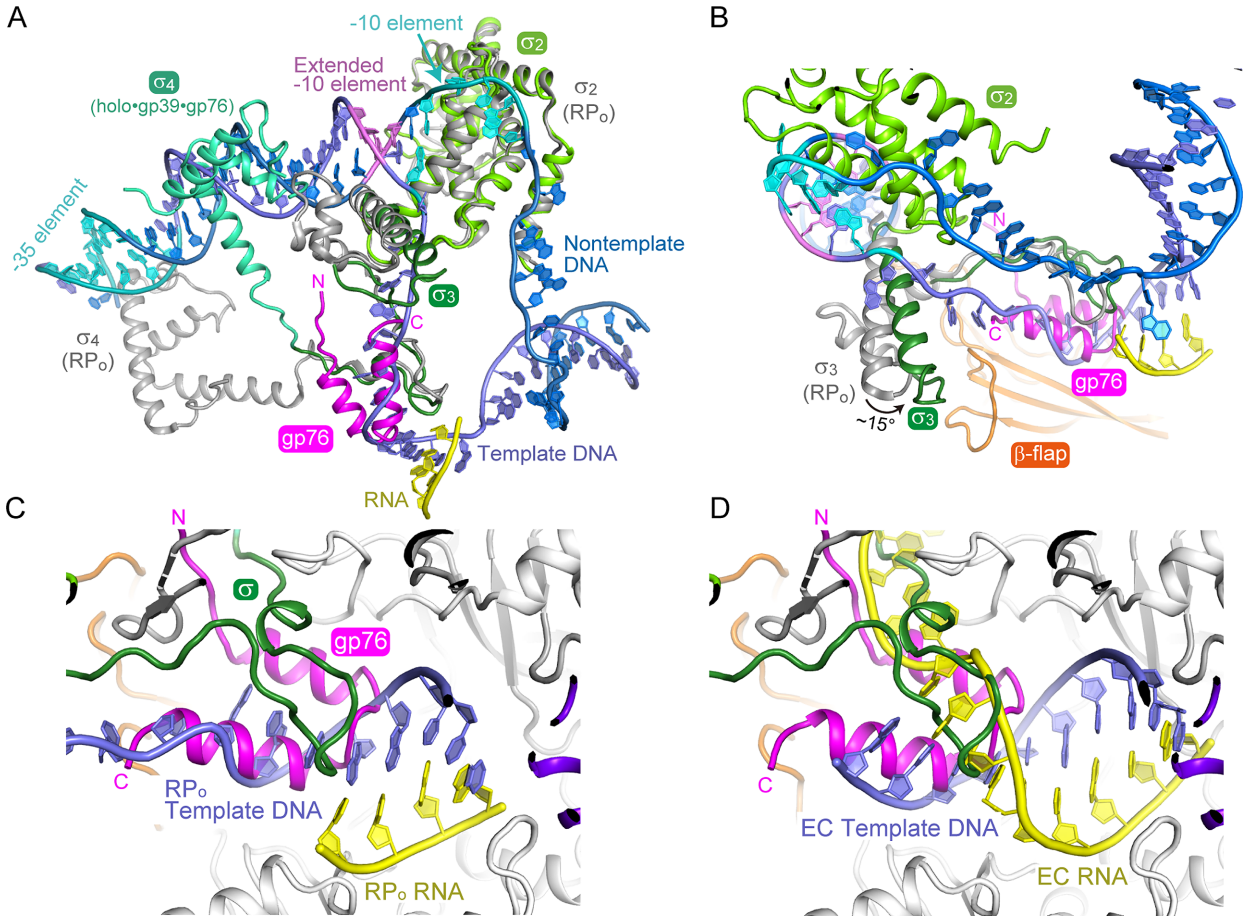

Figure 2. gp76 binding is incompatible with RP_o formation and transcription elongation. (**A**–**C**) Structural comparison with RP_o. The structure of *T. aquaticus* RP_o (PDB 4XLN) is superimposed on holo•gp39•gp76 by the σ_2 domain of the σ subunit. (C) A close-up view of the RNAP cleft. (**D**) Structural comparison with the elongation complex. The structure of an elongation complex (PDB 2O5I) is superimposed on holo•gp39•gp76 by their core modules.

moter fragment probes 1 and 3, lacking the template strand segments downstream of the –12 position, and to similar probes 2 and 4, bearing the template strand segments (Figure 5A). The RNAP bindings to probes 1–4 are characterized by dissociation constants ranging from 0.1 nM to 5 nM, and can be readily monitored with the beacon assay (22,31). We observed that gp76 strongly inhibited the RNAP interaction with probes 2 and 4, but only modestly affected the binding to probes 1 and 3 (Figure 5C and D). This result is consistent with the expectations from the current structure, and suggests that gp76 inhibits transcription initiation *via* the inhibition of the RP_o formation.

The inhibitory effect of gp76 on transcription from middle and late phage P23–45 promoters is weaker compared to inhibition of host promoter transcription (12). These phage promoters belong to the extended –10 class with an extra TG(TG) motif preceding the –10 consensus (positions –14 to –17) (12). We assumed that the presence of the TG motif is responsible for the weaker inhibition by gp76. Accordingly, we designed probe 5 by adding the TG motif to probe 2, and examined its binding to RNAP by the beacon assay. Probe 5 was found to significantly bind to RNAP in the presence of gp76 (~37% RNAP occupancy compared with that in the absence of gp76) under conditions where almost no binding by probe 2 was detected (Figure 5E). Thus, the addition of the TG motif increases the promoter affinity to RNAP, which allows the promoter DNA to compete with gp76 for common binding site on RNAP.

Gp76 binding is incompatible with transcription elongation

The structure of holo•gp39•go76 also reveals that the gp76 binding affects the conformations of the $\sigma_{3.2}$ linker and the β′ switch 2 (Supplementary Figure S5). Both regions play essential roles in the RP_o stabilization, the *de novo* initiation of RNA synthesis, and the following steps of promoter and σ dissociation during the transition to an elongation complex (10,32). The presence of gp76 is incompatible with these essential functions. The N-terminal loop of the bound gp76 occupies the RNA exit channel, which should be incompatible with transcription elongation (Figure 2D). Conversely, the establishment of an elongation complex should prevent gp76 binding to RNAP, making transcription resistant to inhibition by gp76. Biochemical analyses support the inferences from the structural analysis. gp76 had no effect on transcription elongation/termination by preformed transcription elongation complexes (Supplementary Figure S8B) under the conditions where it efficiently inhibited transcription initiation from promoters (Supplementary Figure

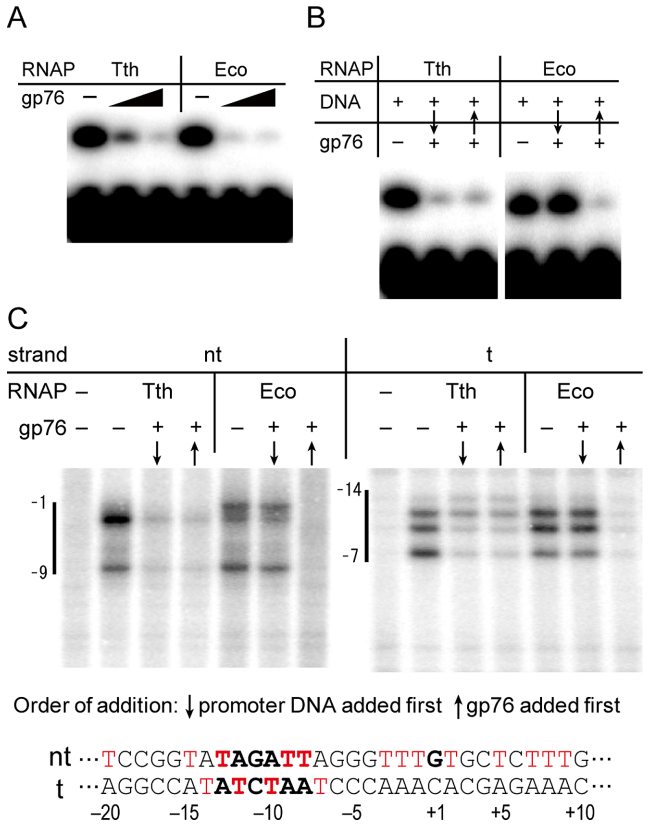

Figure 3. The mechanism of transcription inhibition by gp76. (**A**) Inhibition of transcription initiation by the *T. thermophilus* and *E. coli* RNAP holoenzymes in the presence of gp76 at a –10/-35 promoter (PrpoB2). The concentrations of the RNAPs and the promoter DNA fragment were 100 and 50 nM, respectively. The gp76 concentrations were 1 and 4 μM. (**B**) Analysis of transcription inhibition by gp76 added to the reaction either before or after the promoter DNA; arrows indicate the order of addition between the promoter DNA and gp76. The gp76 concentration was 4 μM. (**C**) Analysis of promoter melting in the presence of gp76, using $KMnO_4$ probing. Thymine positions in the melted region are shown for each DNA strand relative to the transcription start site. The sequences of the –10 promoter element and the transcription start site (the G residue) are indicated in bold letters.

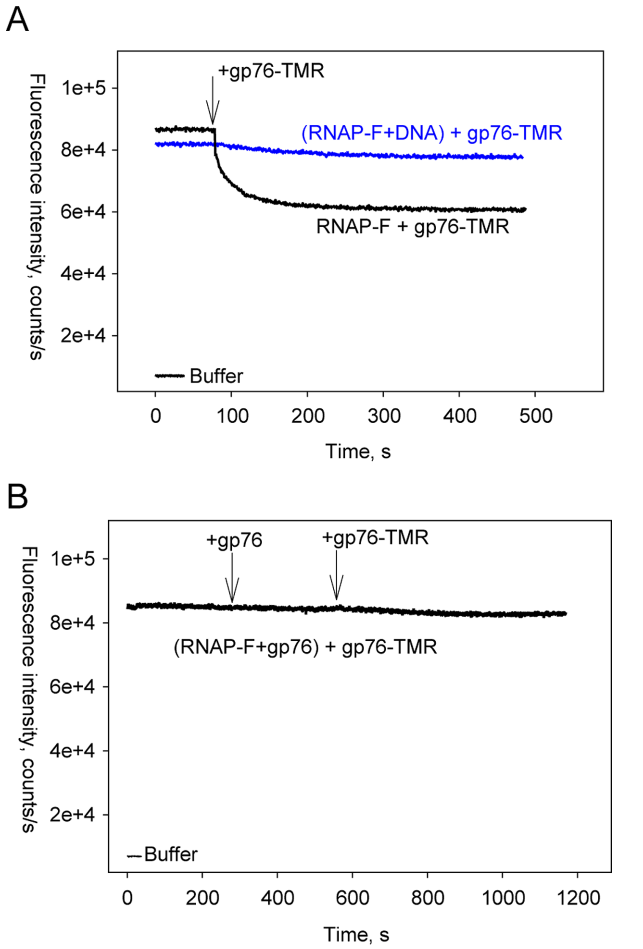

Figure 4. gp76 cannot bind to a stable open complex. (**A**) The gp76 binding to *E. coli* holoenzyme was monitored by measuring FRET between a fluorescein probe incorporated in the σ^{70} subunit and a TMR probe attached to the N-terminus of gp76 (RNAP-F and gp76-TMR, respectively). Quenching of the RNAP-F fluorescence was monitored with or without RNAP-F preincubation with N25cons promoter DNA. The concentrations of RNAP-F, DNA and gp76-TMR were 1, 5 and 150 nM, respectively. (**B**) In control experiment, addition of gp76-TMR to the RNAP-F preincubated with unlabeled gp76 for 5 min caused no change in fluorescence. This confirms the specificity of fluorescence quenching observed in this experiment.

S8A). This is in contrast to gp39, a bifunctional transcription factor, which affects both the promoter specificity and transcription processivity by binding to the outside surface of the RNAP β-flap (Supplementary Figure S8B) (20).

DISCUSSION

Bacteriophages employ a wide array of mechanisms to manipulate bacterial biological processes for their own developmental needs during infection. The *T. thermophilus* bacteriophage P23–45 evolved unique infection mechanisms for transcription of its early, middle, and late genes (12). While the early genes are transcribed by the phage-encoded RNAP, the middle and late genes depend on the host RNAP for transcription. The phage employs two protein factors, gp76 (an early gene product) and gp39 (a middle gene product), which bind to the host RNAP to shut off the host-gene transcription, while minimally affecting the phage-gene transcription. Given the times of the maximal expression of their genes, gp76 should appear earlier in infected cells, and bind to the host RNAP holoenzyme first to form holo•76, with subsequent binding of gp39 to form holo•gp39•gp76.

In our previous study, we reported the structure of holo•gp39 (13). In the structure, gp39 binds to the outside face of the RNAP β-flap, and relocates the σ_4 domain of the σ^A subunit, which is responsible for the recognition of the promoter –35 element (13). The σ_4 relocation is incompatible with the concurrent binding of σ_2 and σ_4 to the promoter –10 and –35 elements, respectively, leading to the inhibition of the transcription of host genes controlled by the major –10/–35 class promoters. In contrast, the transcription of genes controlled by the minor extended –10 class promoters (not relying on the –35 element) should be minimally affected, and the phage middle and late promoters belong to this class.

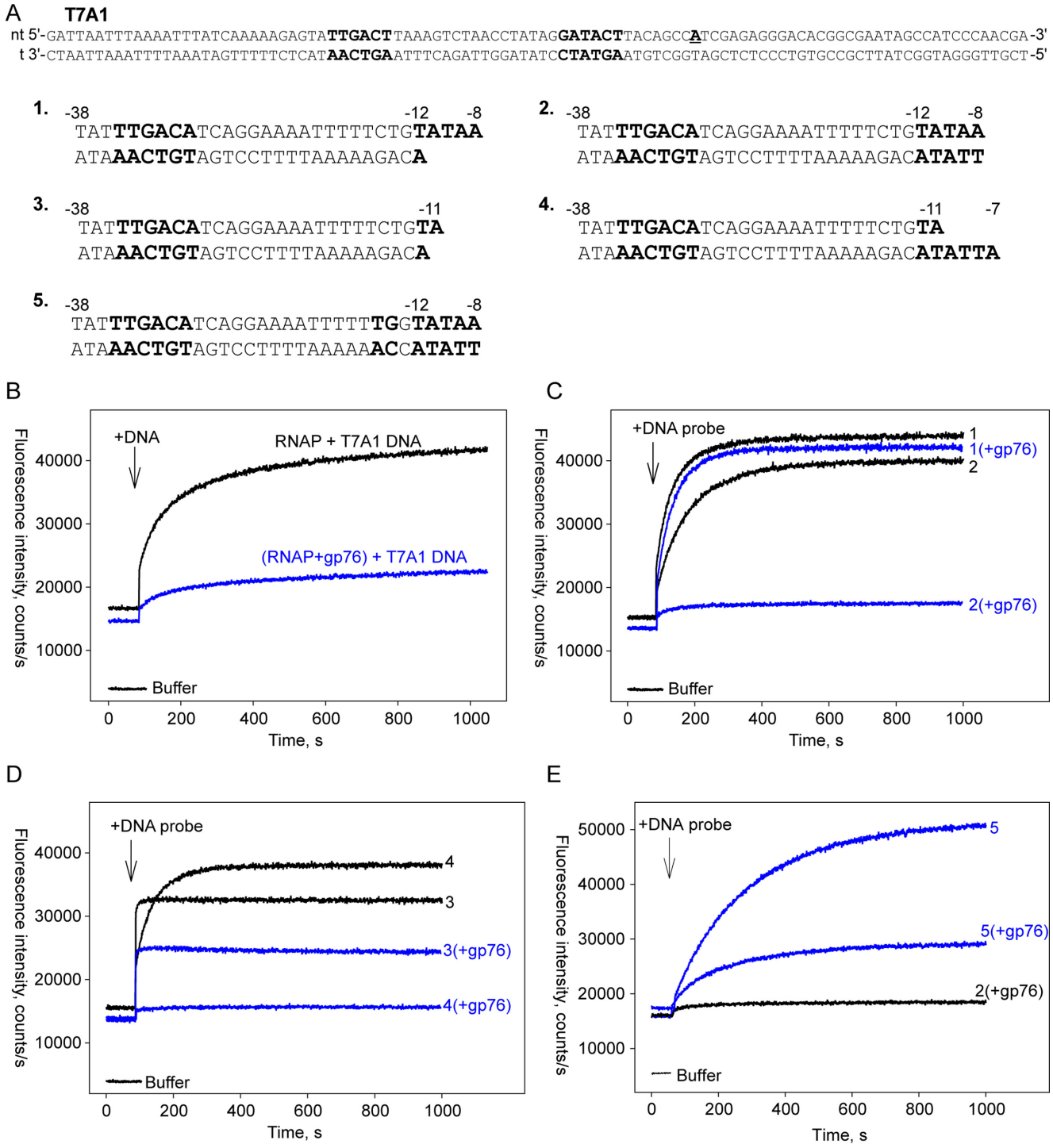

Figure 5. The effect of gp76 on RNAP beacon binding to promoter fragment probes. (**A**) Nucleotide sequences of the DNA fragments. The –10 and –35 promoter elements are highlighted in bold letters. The transcription start site is indicated as an underlined bold letter. (**B**–**E**) The *E. coli* RNAP beacon (1 nM) with or without 150 nM gp76 was mixed with either (B) 4 nM T7 A1 promoter fragment (–65 to +35), (C) 2 nM DNA probes 1 and 2, (D) DNA probes 3 (10 nM) and 4 (2 nM) or (E) 2 nM DNA probes 2 and 5, respectively lacking and bearing the TG motif, and increases in fluorescence were monitored. Note that, in the absence of gp76, probe 4 shows ∼20-fold higher affinity for RNAP, as compared to probe 3 (K_D values are 0.24 and 5.3 nM, respectively (31)).

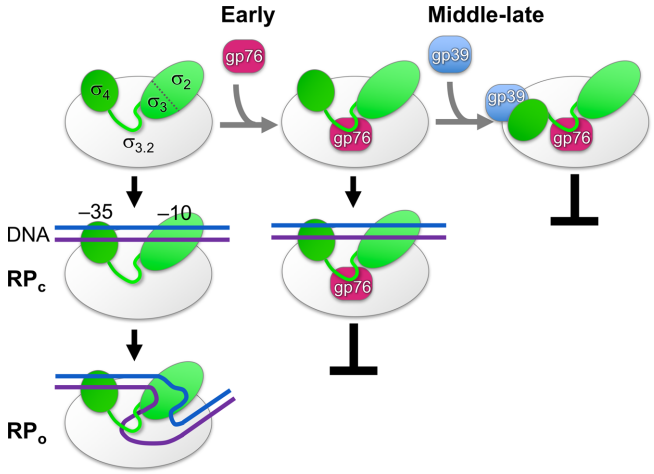

Figure 6. Mechanism of RNAP appropriation by the phage proteins. A cartoon depicting how gp76 and gp39 of the P23–45 phage hijack transcription initiation by the host RNAP. gp76 is an early gene product, and first binds to the RNAP holoenzyme in this model. It occludes the template-strand DNA binding site within the RNAP cleft, and sterically hinders the RP_o formation. gp39 is a middle gene product, and later participates in the preformed holo•gp76. gp39 binds near the RNA exit site, and relocates the –35 recognition domain (σ_4) of the σ subunit to compromise the promoter recognition, leading to stricter suppression of the host gene transcription.

In the present study, we solved the structure of holo•gp39•gp76. The structure revealed that gp76 binds within the RNAP cleft as a nucleic acid mimic. It occludes the template-strand DNA binding site in the main channel, as well as the RNA exit channel, and sterically hinders the RP_o formation (Figure 6). gp76 and gp39 bind on mutually opposite sides of the RNAP β-flap, and inhibit transcription *via* completely different mechanisms. While gp76 blocks the functions of the σ_2/σ_3 regions for the RP_o formation, gp39 relocates σ_4 to compromise the –35 recognition. During the course of infection, gp39 should bind the previously established holo•gp76, which is resistant to the RP_o formation, and then alter the promoter preference with regard to the –35 element for the stricter suppression of the host gene transcription (from the –10/–35 class genes) (Figure 6). It may also contribute to a switch from middle to late phage transcription.

Although gp76 suppresses the transcription of the host genes transcribed from the –10/–35 class promoters, its inhibitory effect is weaker on the middle and late phage promoters belonging to the extended –10 class (12). The extended –10 element forms sequence-specific interactions with both σ_2 and the β′-zipper (7,33,34). As revealed by the beacon assay, these extra interactions increase the promoter affinity to the RNAP at the point of DNA melting, possibly increasing the lifetime of the melted DNA strands. As gp76 occupies the natural path of the DNA template strand at positions –11 to –4 (Figure 2A–C), the propagation of the DNA melting beyond position –11 and the complete accommodation of the template DNA within the active site would require the dissociation of the bound gp76. The higher DNA-RNAP affinity conferred by the extended –10 element extra interactions should contribute to the efficient competition of DNA for the common binding site with gp76, and this could be the basis of the differential effects on different promoter classes.

The inhibition mechanism by gp76 is reminiscent of those by a class of antibiotics including myxopyronin, lipiarmycin, ripostatin, and corallopyronin (35–38). These antibiotics specifically bind near the β′ switch 2 of RNAP, the putative hinge that mediates the opening and closing of the RNAP clamp, and inhibit the RP_o formation by interfering with the DNA template strand loading to the RNAP active center (36). In the structure of the myxopyronin-bound RNAP holoenzyme (35,38), the antibiotic binds in a hydrophobic pocket formed by the β′ switch 2 and the adjacent parts of the clamp. The antibiotic binding results in a conformational change in the β′ switch 2, and indirectly hinders the template strand loading, probably by interfering with the clamp opening. As compared with the current holo•gp39•gp76 structure, the binding site of gp76 is distinct from that of myxopyronin, and gp76 appears to directly inhibit the RP_o formation by sterically blocking the DNA loading. Thus, the present structure provides a new structural platform for the future development of potent antibacterial drugs.

AVAILABILITY

Atomic coordinates and structure factors for the reported crystal structures have been deposited with the Protein Data bank under accession number 5XJ0.

SUPPLEMENTARY DATA

Supplementary Data are available at NAR online.

ACKNOWLEDGEMENTS

We thank T. Uejima, H. Shimizu, H. Ehara and T. Ito for helpful discussion and assistance. The synchrotron radiation experiments were performed at BL41XU of SPring-8 with the approval of the Japan Synchrotron Radiation Research Institute (Proposal Nos. 2014B1265, 2015B2040, 2016A2526, 2016B2526), and at NE3A of the Photon Factory with the approval of the Photon Factory Program Advisory Committee (Proposal No. 2015G520).

FUNDING

Japan Society for the Promotion of Science KAKENHI [JP23370048 and JP15H04344 to S.S.]; National Institutes of Health [RO1 GM59295 to K.S.]; Ministry of Education and Science of the Russian Federation [14.B25.31.0004 to K.S.]. Funding for open access charge: JSPS KAKENHI.
Conflict of interest statement. None declared.

REFERENCES

1. Vassylyev,D.G., Sekine,S., Laptenko,O., Lee,J., Vassylyeva,M.N., Borukhov,S. and Yokoyama,S. (2002) Crystal structure of a bacterial RNA polymerase holoenzyme at 2.6 A resolution. *Nature*, **417**, 712–719.
2. Murakami,K.S., Masuda,S. and Darst,S.A. (2002) Structural basis of transcription initiation: RNA polymerase holoenzyme at 4 A resolution. *Science*, **296**, 1280–1284.

3. Saecker,R.M., Record,M.T. Jr and Dehaseth,P.L. (2011) Mechanism of bacterial transcription initiation: RNA polymerase - promoter binding, isomerization to initiation-competent open complexes, and initiation of RNA synthesis. *J. Mol. Biol.*, **412**, 754–771.
4. Feklistov,A., Barinova,N., Sevostyanova,A., Heyduk,E., Bass,I., Vvedenskaya,I., Kuznedelov,K., Merkiene,E., Stavrovskaya,E., Klimasauskas,S. *et al.* (2006) A basal promoter element recognized by free RNA polymerase sigma subunit determines promoter recognition by RNA polymerase holoenzyme. *Mol. Cell*, **23**, 97–107.
5. Feklistov,A. and Darst,S.A. (2011) Structural basis for promoter-10 element recognition by the bacterial RNA polymerase sigma subunit. *Cell*, **147**, 1257–1269.
6. Campbell,E.A., Muzzin,O., Chlenov,M., Sun,J.L., Olson,C.A., Weinman,O., Trester-Zedlitz,M.L. and Darst,S.A. (2002) Structure of the bacterial RNA polymerase promoter specificity sigma subunit. *Mol. Cell*, **9**, 527–539.
7. Bae,B., Feklistov,A., Lass-Napiorkowska,A., Landick,R. and Darst,S.A. (2015) Structure of a bacterial RNA polymerase holoenzyme open promoter complex. *Elife*, **4**, doi:10.7554/eLife.08504.
8. Zuo,Y. and Steitz,T.A. (2015) Crystal structures of the E. coli transcription initiation complexes with a complete bubble. *Mol. Cell*, **58**, 534–540.
9. Zhang,Y., Feng,Y., Chatterjee,S., Tuske,S., Ho,M.X., Arnold,E. and Ebright,R.H. (2012) Structural basis of transcription initiation. *Science*, **338**, 1076–1080.
10. Pupov,D., Kuzin,I., Bass,I. and Kulbachinskiy,A. (2014) Distinct functions of the RNA polymerase sigma subunit region 3.2 in RNA priming and promoter escape. *Nucleic Acids Res.*, **42**, 4494–4504.
11. Minakhin,L., Goel,M., Berdygulova,Z., Ramanculov,E., Florens,L., Glazko,G., Karamychev,V.N., Slesarev,A.I., Kozyavkin,S.A., Khromov,I. *et al.* (2008) Genome comparison and proteomic characterization of Thermus thermophilus bacteriophages P23-45 and P74-26: siphoviruses with triplex-forming sequences and the longest known tails. *J. Mol. Biol.*, **378**, 468–480.
12. Berdygulova,Z., Westblade,L.F., Florens,L., Koonin,E.V., Chait,B.T., Ramanculov,E., Washburn,M.P., Darst,S.A., Severinov,K. and Minakhin,L. (2011) Temporal regulation of gene expression of the Thermus thermophilus bacteriophage P23-45. *J. Mol. Biol.*, **405**, 125–142.
13. Tagami,S., Sekine,S., Minakhin,L., Esyunina,D., Akasaka,R., Shirouzu,M., Kulbachinskiy,A., Severinov,K. and Yokoyama,S. (2014) Structural basis for promoter specificity switching of RNA polymerase by a phage factor. *Genes Dev.*, **28**, 521–531.
14. Vassylyeva,M.N., Lee,J., Sekine,S.I., Laptenko,O., Kuramitsu,S., Shibata,T., Inoue,Y., Borukhov,S., Vassylyev,D.G. and Yokoyama,S. (2002) Purification, crystallization and initial crystallographic analysis of RNA polymerase holoenzyme from Thermus thermophilus. *Acta Crystallogr. D Biol. Crystallogr.*, **58**, 1497–1500.
15. Van Duyne,G.D., Standaert,R.F., Karplus,P.A., Schreiber,S.L. and Clardy,J. (1993) Atomic structures of the human immunophilin FKBP-12 complexes with FK506 and rapamycin. *J. Mol. Biol.*, **229**, 105–124.
16. Otwinowski,Z. and Minor,W. (1997) Processing of X-ray diffraction data collected in oscillation mode. *Methods Enzymol.*, **276**, 307–326.
17. McCoy,A.J., Grosse-Kunstleve,R.W., Adams,P.D., Winn,M.D., Storoni,L.C. and Read,R.J. (2007) Phaser crystallographic software. *J. Appl. Crystallogr.*, **40**, 658–674.
18. Emsley,P., Lohkamp,B., Scott,W.G. and Cowtan,K. (2010) Features and development of Coot. *Acta Crystallogr. D Biol. Crystallogr.*, **66**, 486–501.
19. Adams,P.D., Afonine,P.V., Bunkoczi,G., Chen,V.B., Davis,I.W., Echols,N., Headd,J.J., Hung,L.W., Kapral,G.J., Grosse-Kunstleve,R.W. *et al.* (2010) PHENIX: a comprehensive Python-based system for macromolecular structure solution. *Acta Crystallogr. D Biol. Crystallogr.*, **66**, 213–221.
20. Berdygulova,Z., Esyunina,D., Miropolskaya,N., Mukhamedyarov,D., Kuznedelov,K., Nickels,B.E., Severinov,K., Kulbachinskiy,A. and Minakhin,L. (2012) A novel phage-encoded transcription antiterminator acts by suppressing bacterial RNA polymerase pausing. *Nucleic Acids Res.*, **40**, 4052–4063.
21. Mekler,V., Minakhin,L., Sheppard,C., Wigneshweraraj,S. and Severinov,K. (2011) Molecular mechanism of transcription inhibition by phage T7 gp2 protein. *J. Mol. Biol.*, **413**, 1016–1027.
22. Mekler,V., Pavlova,O. and Severinov,K. (2011) Interaction of Escherichia coli RNA polymerase sigma70 subunit with promoter elements in the context of free sigma70, RNA polymerase holoenzyme, and the beta'-sigma70 complex. *J. Biol. Chem.*, **286**, 270–279.
23. Mekler,V. and Severinov,K. (2015) RNA polymerase molecular beacon as tool for studies of RNA polymerase-promoter interactions. *Methods*, **86**, 19–26.
24. Knight,J.L., Mekler,V., Mukhopadhyay,J., Ebright,R.H. and Levy,R.M. (2005) Distance-restrained docking of rifampicin and rifamycin SV to RNA polymerase using systematic FRET measurements: developing benchmarks of model quality and reliability. *Biophys. J.*, **88**, 925–938.
25. Tagami,S., Sekine,S., Kumarevel,T., Hino,N., Murayama,Y., Kamegamori,S., Yamamoto,M., Sakamoto,K. and Yokoyama,S. (2010) Crystal structure of bacterial RNA polymerase bound with a transcription inhibitor protein. *Nature*, **468**, 978–982.
26. Sekine,S., Murayama,Y., Svetlov,V., Nudler,E. and Yokoyama,S. (2015) The ratcheted and ratchetable structural states of RNA polymerase underlie multiple transcriptional functions. *Mol. Cell*, **57**, 408–421.
27. Sekine,S., Murayama,Y., Svetlov,V., Nudler,E. and Yokoyama,S. (2015) Ratcheting of RNA polymerase toward structural principles of RNA polymerase operations. *Transcription*, **6**, 56–60.
28. Murakami,K.S., Masuda,S., Campbell,E.A., Muzzin,O. and Darst,S.A. (2002) Structural basis of transcription initiation: an RNA polymerase holoenzyme-DNA complex. *Science*, **296**, 1285–1290.
29. Xue,Y., Hogan,B.P. and Erie,D.A. (2000) Purification and initial characterization of RNA polymerase from Thermus thermophilus strain HB8. *Biochemistry*, **39**, 14356–14362.
30. Miropolskaya,N., Ignatov,A., Bass,I., Zhilina,E., Pupov,D. and Kulbachinskiy,A. (2012) Distinct functions of regions 1.1 and 1.2 of RNA polymerase sigma subunits from Escherichia coli and Thermus aquaticus in transcription initiation. *J. Biol. Chem.*, **287**, 23779–23789.
31. Mekler,V. and Severinov,K. (2013) Cooperativity and interaction energy threshold effects in recognition of the -10 promoter element by bacterial RNA polymerase. *Nucleic Acids Res.*, **41**, 7276–7285.
32. Pupov,D., Miropolskaya,N., Sevostyanova,A., Bass,I., Artsimovitch,I. and Kulbachinskiy,A. (2010) Multiple roles of the RNA polymerase β' SW2 region in transcription initiation, promoter escape, and RNA elongation. *Nucleic Acids Res.*, **38**, 5784–5796.
33. Keilty,S. and Rosenberg,M. (1987) Constitutive function of a positively regulated promoter reveals new sequences essential for activity. *J. Biol. Chem.*, **262**, 6389–6395.
34. Yuzenkova,Y., Tadigotla,V.R., Severinov,K. and Zenkin,N. (2011) A new basal promoter element recognized by RNA polymerase core enzyme. *EMBO J.*, **30**, 3766–3775.
35. Mukhopadhyay,J., Das,K., Ismail,S., Koppstein,D., Jang,M., Hudson,B., Sarafianos,S., Tuske,S., Patel,J., Jansen,R. *et al.* (2008) The RNA polymerase "switch region" is a target for inhibitors. *Cell*, **135**, 295–307.
36. Srivastava,A., Talaue,M., Liu,S., Degen,D., Ebright,R.Y., Sineva,E., Chakraborty,A., Druzhinin,S.Y., Chatterjee,S., Mukhopadhyay,J. *et al.* (2011) New target for inhibition of bacterial RNA polymerase: 'switch region'. *Curr. Opin. Microbiol.*, **14**, 532–543.
37. Tupin,A., Gualtieri,M., Leonetti,J.P. and Brodolin,K. (2010) The transcription inhibitor lipiarmycin blocks DNA fitting into the RNA polymerase catalytic site. *EMBO J.*, **29**, 2527–2537.
38. Belogurov,G.A., Vassylyeva,M.N., Sevostyanova,A., Appleman,J.R., Xiang,A.X., Lira,R., Webber,S.E., Klyuyev,S., Nudler,E., Artsimovitch,I. *et al.* (2009) Transcription inactivation through local refolding of the RNA polymerase structure. *Nature*, **457**, 332–335.